Dirac R-matrix calculations of photoionization cross sections of Ni XII and atomic structure data of Ni XIII

R T Nazir†, M A Bari, M Bilal, S Sardar, M H Nasim, and M Salahuddin

Department of Physics and Applied Mathematics, Pakistan Institute of Engineering and Applied Sciences, Islamabad 45650, *Pakistan*

(Received 11 August 2016; revised manuscript received 26 October 2016; published online 20 December 2016)

We performed R-matrix calculations for photoionization cross sections of the two ground state configuration $3s^2 3p^5$ ($^2P^o_{3/2,1/2}$) levels and 12 excited states of Ni XII using relativistic Dirac Atomic R-matrix Codes (DARC) across the photon energy range between the ionizations thresholds of the corresponding states and well above the thresholds of the last level of the Ni XIII target ion. Generally, a good agreement is obtained between our results and the earlier theoretical photoionization cross sections. Moreover, we have used two independent fully relativistic GRASP and FAC codes to calculate fine-structure energy levels, wavelengths, oscillator strengths, transitions rates among the lowest 48 levels belonging to the configuration ($3s^2 3p^4$, $3s3p^5$, $3p^6$, $3s^2 3p^3 3d$) in Ni XIII. Additionally, radiative lifetimes of all the excited states of Ni XIII are presented. Our results of the atomic structure of Ni XIII show good agreement with other theoretical and experimental results available in the literature. A good agreement is found between our calculated lifetimes and the experimental ones. Our present results are useful for plasma diagnostic of fusion and astrophysical plasmas.

Keywords: photoionization cross sections, energy levels, wavelengths, lifetimes

PACS: 31.15.ag, 31.15.aj, 31.15.am, 32.80.–t **DOI:** 10.1088/1674-1056/26/2/023102

1. Introduction

The interaction of photons with atoms or ions is a fundamental atomic process in nature to obtain information about the structure and dynamics of astrophysical objects. As much of this immense universe is in ionic form, photoabsorption and photoionization (PI) are used for spectral modeling of astrophysical plasmas.[1,2] The modeling of detailed balancing between ionization and thermal processes for astrophysical interpretations and modeling of laboratory plasmas require reliable PI cross-sections for all astrophysically abundant elements, in all ionization stages and for all bound electrons.[3] Several efforts have been made to investigate PI cross sections both on experimental and theoretical fronts. The Opacity Project (OP)[4] is an online atomic database which provides PI cross sections which are often useful for the plasma modeling community, but when accurate data are absent hydrogenic approximations are used. To the best of our knowledge, no theoretical PI cross section calculations for Ni XII including the excited (metastable) states of this ion are available in the literature; they are limited to the ground state only.[2] Accurate PI cross sections are required for this ion and various ionization stages of Ni to solve the problem of solar opacity. The R-matrix scattering calculations for the electron collisional excitation of Ni XII has recently been reported by Del Zanna *et al.*[5]

Nickel is the most abundant transition element existing in different ionization stages in the sun and other astrophysical plasmas after iron. As Ni emission lines have been detected in the spectra of a variety of astronomical objects such as black hole x-ray binaries,[6,7] clusters of galaxies,[8] supernova remnants,[9] and the center of our Galaxy.[10] Solar emission lines from Ni XII are prominent in the soft x-rays and EUV part[11] of the spectrum. Several forbidden coronal lines are observed in the visible and UV region of the solar spectrum.[12] In a similar way, extreme ultraviolet (EUV) emission lines from $n = 3$–3 transitions in Ni XIII ions have been observed in the spectra of the Sun and many solar-type stars.[13,14] Since Ni is an important impurity element in the JET tokamak (from both divertor and limiter configurations) fusion reactor and M-shell emission spectra in the 14.4 nm–16.5 nm from five K-like Ni^{9+} to P-like Ni^{13+} ions have been described by Mattioli *et al.*[15] both experimentally and theoretically. These EUV emission lines have also been observed in a beam-foil experiment in laboratory plasma.[16]

The Ni XII ion belongs to the chlorine isoelectronic sequence, and PI cross sections along this sequence are scarce in the literature owing to the complexity in strong electron-electron interactions. Over the last few decades, experimental measurements[17–22] of the PI cross section of ions of the Cl-like sequence made by a number of workers have been described by Alna'washi *et al.*[23] in a joint experimental and theoretical work about the valence-shell PI of Cl-like Ca IV ions. Recently, Tyndall *et al.*[24] reported valence and L-shell PI cross sections of Ar II using the relativistic Dirac Atomic R-matrix Codes (DARC).

We also report here the atomic structure data of energy levels, wavelengths, oscillator strengths, and transitions rates

†Corresponding author. E-mail: rajatariq20@gmail.com

© 2017 Chinese Physical Society and IOP Publishing Ltd

of the Ni XIII target ion using the fully relativistic GRASP code[25] as well as the Flexible Atomic Code (FAC)[26] which yields results comparable to GRASP. Results from FAC are helpful in assessing the accuracy of our energy levels and radiative data of Ni XIII. Finally, results of radiative lifetimes of excited levels of Ni XIII obtained using GRASP and FAC codes are given in Table 3. We have computed radiative data for all the electric dipole (E1), magnetic dipole (M1), electric quadrupole (E2), and magnetic quadrupole (M2) transition between the four main configurations ($3s^23p^4$, $3s3p^5$, $3s^23p^33d$, $3p^6$) by taking CI effects among 6 even parity ($3s^23p^4$, $3p^6$, $3s^23p^23d^2$, $3s3p^43d$, $3s^23p^34p$, $3s^23p^34f$) and 7 odd-parity ($3s3p^5$, $3s^23p^33d$, $3s3p^33d^2$, $3p^53d$, $3s^23p3d^3$, $3s^23p^34s$, $3s^23p^34d$) configurations. The above 13 configurations give rise to 735 fine-structure levels. Our FAC predicted lifetimes are computed from the transition rates of all the possible four types of transitions (E1, E2, M1, M2). In our GRASP lifetime calculations, we retained three types of transitions (E1, E2, M1) due to computational constraints.

Over the past few years, many approaches have been applied to calculate energy levels, oscillator strengths, transition rates and lifetimes for Ni XIII. Fawcett[27] calculated energy levels, wavelengths, oscillator strengths of Ni XIII with the Hartree–Fock relativistic (HFR) approach using a set of $3s^23p^4$, $3s3p^5$ and $3s^23p^33d$ configurations. Chou *et al.*[28] reported energy levels and transition rates among five levels of the ground configuration of S-like ions with the multi-configuration Dirac–Fock (MCDF) technique[25] by excluding the $3p^6$ ($^1S_0$) configuration. Bhatia *et al.*[29] calculated 48 fine-structures of Ni XIII with the superstructure (SS) code.[30] To date the best available calculations of energy levels and transitions rates in Ni XIII were carried out by Aggarwal[31] with the GRASP (General purpose Relativistic Atomic Structure Program) code[25] using a set of 12 configurations. In our calculations we found significant improvement in the level energies of $3s^23p^33d$ by including an additional configuration $3s^23p3d^3$ than the atomic model of Ref. [31].

Ishikawa and Vilkas[32] calculated energy levels, wavelengths, and transition rates of optically allowed transitions among 46 levels arising from the $3s^23p^4$, $3s3p^5$, and $3s^23p^33d$ configurations of S-like ions ($Z = 26$–32) using Multireference Møller–Plesset (MR-MP) perturbation theory. Froese Fischer[33] reported transition rates between levels of the ground configuration $3p^4$ of the Ni XIII ion using the multi-configuration Dirac–Hartree–Fock (MCDHF) method[34] implemented in the GRASP2K computer program.[35] Most of these previous calculations are restricted to the wavefunction expansion of four main ($3s^23p^4$, $3s3p^5$, $3s^23p^33d$, $3p^6$) configurations of the $n = 3$ complex. Moreover, these studies investigated atomic parameters only for allowed transitions (E1). The experimental measurements of spectral data for various highly ionized Ni ions (Ni IX–Ni XXVII) have been critically reviewed and tabulated by Shirai *et al.*[36]

In this paper we present large scale calculations for PI cross sections of Ni XII, along with atomic structure parameters of Ni XIII target ion. The fully relativistic Dirac atomic R-matrix code (DARC)[37] is employed to study the PI process of Ni XII for the two ground and 12 metastable states. Our present results for the ground state configuration $3s^23p^5$ ($^2P_{3/2}$, $^2P_{1/2}$) levels are in good agreement with previous theoretical work.[38] Our calculated ionization threshold energies are in excellent agreement with those available in the NIST tabulation. Furthermore, no theoretical results on the PI cross sections are available for the meta-stable states in the Ni XII ion. Finally, we have used fully relativistic GRASP and FAC codes to study energy levels, wavelengths, oscillator strengths, transition rates, and lifetimes of Ni XIII. Where possible we have compared our results with the available experimental and theoretical data in order to assess the accuracy of our present work for applications.

2. Methods of calculations

2.1. Photoionization cross sections

To carry out PI cross section calculations of Ni XII, we have used the DARC code based on the fully relativistic R-matrix method. We have adopted the same methodology as discussed in Ref. [39]. The atomic system is represented by a 'target' or the core of the N-electrons system interacting with the $(N+1)$-th electron. In this method, the Dirac Hamiltonian for the $(N+1)$-electron system can be expressed in atomic units (a.u.) as

$$H^{N+1} = \sum_{i=1}^{N+1} -\mathrm{i}c\alpha\cdot\nabla_i + (\beta-1)c^2 - \frac{Z}{r_i} + \sum_{j=i+1}^{N+1}\frac{1}{|r_j - r_i|}, \quad (1)$$

where i and j represent the individual electrons and summation runs over all electrons of the system. The usual Dirac matrices α and β are constructed using Pauli spin and unit matrices.

Prior to the R-matrix calculations, the target wavefunction is obtained from the multi-configurational Dirac–Fock code GRASP by using an extended average level (EAL) optimizing scheme for the target ion states involved in the present calculations. The 48-state wavefunction expansion belonging to the four main configurations ($3s^23p^4$, $3s3p^5$, $3s^23p^33d$, $3p^6$) up to $n = 3$ levels is selected which entails the dominant dipole transitions in the core ion and important correlation effects. The calculated 48 energy levels are compared with experimental energies and other theoretical results in Table 1.

Table 1. Comparison of energy levels (in unit Ryd) of Ni XIII and their radiative lifetimes (in unit s). The number form expression $a \pm b \equiv a \times 10^{\pm b}$.

			Energies							Lifetimes	
Index	Config.	Term	GRASP1	FAC	NIST	HFR	SS	GRASP	MR-MP	τ_g	τ_f
1	$3s^2 3p^4$	$^3P_2$	0.000	0.000	0.000	0.000	0.000	0.000	0.000	–	–
2		$^3P_1$	0.176	0.176	0.178	0.172	0.163	0.176	0.178	6.55 –03	6.59 –03
3		$^3P_0$	0.183	0.182	0.183	0.181	0.169	0.183	0.183	2.21+01	1.95+01
4		$^1D_2$	0.445	0.443	0.429	0.413	0.444	0.445	0.428	3.51 –03	3.55 –03
5		$^1S_0$	0.900	0.896	0.892	0.891	0.828	0.899	0.890	3.85 –04	3.93 –04
6	$3s3p^5$	$^3P_2$	2.974	2.986	3.009	3.009	2.918	3.002	3.012	2.62 –10	2.53 –10
7		$^3P_1$	3.102	3.113	3.136	3.132	3.038	3.130	3.139	2.41 –10	2.33 –10
8		$^3P_0$	3.186	3.198		3.214	3.115	3.214	3.224	2.46 –10	2.37 –10
9		$^1P_1$	3.856	3.861	3.836	3.831	3.763	3.889	3.835	9.05 –11	8.85 –11
10	$3s^2 3p^3 3d$	$^5D_0$	4.083	4.085		4.062	3.975	4.113	4.081	4.58 –09	4.45 –09
11		$^5D_1$	4.086	4.088		4.066	3.979	4.116	4.084	4.59 –09	4.45 –09
12		$^5D_2$	4.088	4.090		4.068	3.983	4.118	4.086	7.29 –09	7.09 –09
13		$^5D_3$	4.092	4.094		4.073	3.989	4.123	4.090	2.00 –08	1.97 –08
14		$^5D_4$	4.107	4.110		4.090	4.006	4.139	4.106	1.72 –02	1.72 –02
15		$^3D_2$	4.354	4.353		4.315	4.396	4.388	4.327	8.67 –09	8.48 –09
16		$^3D_3$	4.402	4.401		4.362	4.434	4.429	4.378	2.28 –07	2.39 –07
17		$^3D_1$	4.424	4.424		4.382	4.350	4.448	4.400	1.29 –08	1.26 –08
18		$^3F_2$	4.478	4.477		4.438	4.286	4.528	4.448	1.59 –08	1.53 –08
19		$^1S_0$	4.515	4.515		4.476	4.490	4.537	4.481	8.99 –09	8.80 –09
20		$^3F_3$	4.519	4.517		4.477	4.329	4.572	4.488	2.41 –08	2.37 –08
21		$^3F_4$	4.579	4.577		4.535	4.491	4.632	4.547	7.01 –03	3.88 –03
22		$^3G_3$	4.768	4.764		4.684	4.648	4.821	4.706	4.43 –09	4.32 –09
23		$^3G_4$	4.794	4.790		4.711	4.675	4.846	4.733	1.08 –02	1.20 –02
24		$^3G_5$	4.830	4.826		4.747	4.705	4.881	4.768	2.90 –02	2.91 –02
25		$^1G_4$	4.894	4.888		4.799	4.785	4.936	4.822	6.41 –03	5.97 –03
26		$^1D_2$	4.958	4.952		4.885	4.886	5.025	4.911	6.49 –10	6.43 –10
27		$^3D_1$	5.093	5.086		4.980	5.020	5.139	5.031	3.62 –10	3.55 –10
28		$^3P_0$	5.107	5.102		5.018	5.065	5.170	5.060	3.97 –09	4.12 –09
29		$^3P_1$	5.136	5.130		5.049	5.095	5.206	5.086	2.02 –10	1.98 –10
30		$^3F_3$	5.166	5.160		5.075	5.100	5.237	5.110	1.69 –09	1.65 –09
31		$^3D_2$	5.174	5.167		5.088	5.094	5.259	5.116	6.05 –09	5.45 –09
32		$^3F_4$	5.199	5.194		5.113	5.130	5.283	5.144	6.35 –04	6.57 –04
33		$^3F_2$	5.208	5.202		5.122	5.121	5.290	5.149	2.64 –10	2.58 –10
34		$^3P_2$	5.265	5.259		5.186	5.223	5.346	5.216	9.33 –11	9.06 –11
35		$^3D_3$	5.308	5.300		5.189	5.225	5.354	5.245	1.47 –09	1.42 –09
36		$^1F_3$	5.620	5.610		5.479	5.546	5.674	5.536	3.49 –10	3.40 –10
37		$^3P_2$	5.648	5.634	5.551	5.535	5.772	5.704	5.553	7.07 –12	7.20 –12
38		$^1P_1$	5.654	5.641		5.543	5.716	5.718	5.556	6.88 –12	6.97 –12
39		$^3S_1$	5.700	5.685		5.580	5.544	5.811	5.584	8.44 –12	8.57 –12
40		$^3P_0$	5.788	5.773		5.691	5.856	5.876	5.688	6.27 –12	6.36 –12
41		$^3P_1$	5.791	5.776		5.687	5.883	5.889	5.692	6.94 –12	7.03 –12
42		$^3D_3$	5.898	5.880	5.777	5.775	5.884	6.023	5.776	6.03 –12	6.17 –12
43		$^3D_2$	5.995	5.978	5.875	5.874	5.976	6.128	5.872	6.18 –12	6.31 –12
44		$^3D_1$	6.055	6.038	5.922	5.935	6.042	6.190	5.934	6.01 –12	6.14 –12
45		$^1D_2$	6.209	6.191	6.069	6.063	6.140	6.363	6.065	7.51 –12	7.66 –12
46		$^1F_3$	6.353	6.332	6.213	6.215	6.372	6.375	6.216	5.46 –12	5.58 –12
47		$^1P_1$	6.656	6.634	6.525	6.527	6.697	6.677	6.525	6.70 –12	6.85 –12
48	$3p^6$	$^1S_0$	6.748	6.750				6.760		9.43 –11	9.29 –11

GRASP1: Present calculations from GRASP code; FAC: Present calculations from FAC code; HFR: Calculations of Fawcett;[27] SS: Superstructure calculations of Bhatia and Doschek;[29] GRASP: Calculations of Aggarwal *et al.*;[31] MR–MP: Calculations of Ishikawa and Vilkas;[32] τ_g: Radiative lifetimes from GRASP; τ_f: Radiative lifetimes from FAC.

Our DARC calculations are performed for total symmetries of $2J \leq 5$ for odd parity and $2J \leq 3$ for both even and odd parities. The R-matrix boundary radius has been determined by code automatically subjected to the condition that all large components have a magnitude less than 10^{-3}. A basis set of 20-continuum orbitals is considered which is sufficiently large to span the energy range covering the thresholds of all levels of target. The ground state with $J^{\pi} = 3/2^{o}$ is constructed from 156 channels. The Hamiltonian matrix has a dimension of the order of 4899 and 1699 bound channels are generated. To describe the resonance features in vivid detail, PI cross sections are computed at 17550 energy points with a suitable energy mesh (0.5 meV). We did not include the radiation damping of autoionization resonances in the present study as it has very small effects on large resonances.

2.2. Atomic structure of Ni XIII

We obtain target state wavefunctions for Ni XIII using the GRASP code which belongs to the multi-configuration Dirac–Fock (MCDF) GRASP family of codes. In the MCDF approach, an atomic state function (ASF) describes the state of an atom or ion and is constructed approximately by a linear combination of configuration state functions (CSFs) with a given parity P and angular momentum (J, M):

$$\Psi_{\alpha}(PJM) = \sum_{r=1}^{n_c} C_r(\alpha)|\gamma_r(PJM), \tag{2}$$

where n_c is the number of CSFs considered in the atomic state functions calculations and C_r is the mixing coefficient which mirrors the number of electron–electron correlations to be considered. The CSFs are the sum of products of single-electron Dirac spinors

$$\phi(r,\theta,\varphi,\sigma) = \frac{1}{r}\begin{pmatrix} P(r)\chi_{\kappa m}(\theta,\varphi,\sigma) \\ \mathrm{i}Q(r)\chi_{-\kappa m}(\theta,\varphi,\sigma) \end{pmatrix}. \tag{3}$$

Here, κ is a relativistic angular quantum number, $P(r)$ and $Q(r)$ are large and small radial components of one-electron wavefunctions on a logarithmic grid and $\chi_{\kappa m}$ is a spinor spherical harmonic in the LSJ coupling scheme. The CSFs are built from antisymmetrized products of a common set of orthonormal orbitals, optimized on the basis of the Dirac–Coulomb Hamiltonian. The radial functions are determined numerically by solving the MCDF equations, which depend upon varying the orbital radial functions or some subsets so as to obtain an optimized energy functional. The wavefunction can be expanded with thousands of CSFs, and usually allow one to obtain a very reasonable description of the level structure and transition properties for many multiple and highly charged ions, even those with open inner shells. In our GRASP calculations, we have adopted an extended average level (EAL) scheme for our self-consistent calculations to calculate the radial wave functions which optimize a weighted trace of the Hamiltonian using level weights proportional to $2J + 1$. This scheme gives a compromise set of atomic orbitals describing closely lying states with moderate accuracy. All excited levels are calculated simultaneously and then Breit interactions and quantum electrodynamic (QED) effects are included to present the energy levels after higher order corrections. The radial wavefunctions are input into the relativistic Dirac R-matrix (DARC) code in a suitable form.

To assess the accuracy and reliability of our computed GRASP energy levels, wavelengths, oscillator strengths, and transition rates among the lowest 48 fine-structure levels, we also perform parallel calculations using the flexible atomic code (FAC). The FAC is also fully relativistic and based on the jj-coupling scheme. The radial wavefunctions for single-electron orbitals are obtained with a self-consistent field method based on the Dirac formulation. The fine-structure energy levels and atomic state wavefunctions are obtained by diagonalizing the Dirac–Coulomb Hamiltonian. Additionally, FAC lifetimes for all excited levels have been calculated from transition rates of four types of transitions, (E1, E2, M1, M2) obtained with the FAC. We hope that our results will be beneficial in fusion plasma research and astrophysical applications.

3. Results and discussion

3.1. Energy levels

For the set of 48 target orbitals, we have considered a basis set of 13 configurations ($3s^23p^4$, $3s3p^5$, $3p^6$, $3s^23p^33d$, $3s3p^33d^2$, $3p^53d$, $3s^23p3d^3$, $3s^23p^23d^2$, $3s3p^43d$, $3s^23p^34l$) which leads to 735 relativistic levels. This eigenfunction expansion is selected such that it includes the dominant dipole transitions in the core and important correlation effects. Since CI effects are important owing to electron correlations in S-like systems.[31,40] Comparison of our calculated energies of the 48 levels belonging to the four main configurations ($3s^23p^4$, $3s3p^5$, $3p^6$, $3s^23p^33d$) with the observed energies and other theoretical energies[27–29,31,32] is presented in Table 1. In this table, the last two columns show the present lifetimes obtained from GRASP and FAC codes.

Our calculated GRASP energies agree with the observed values with an average percent difference of 1.2%, and the maximum difference is 3.7% for the state $3s^2\ 3p^4\ (^1D_2)$. For the levels of ground state configuration ($3s^2\ 3p^4$), our calculated FAC energies agree well with the NIST values within 0.5%–3.3%. The present FAC energy values for the 7 fine-structure levels belonging to the configuration $3s^2\ 3p^33d$ lie closer to the experimental energies within 2.0% as compared to both present and previous GRASP calculations,[31] which

are nearly 4%–5% higher than the NIST values. The maximum disagreement between our calculated GRASP and FAC energies is about 0.5% for the $3s^2\ 3p^4\ {}^3P_0$ level and both calculations are consistent with each other. Table 1 shows that our FAC energies lie closer to the experimental values within 3.2% as compared to GRASP energies, which show a maximum discrepancy of 3.7%. Our present FAC results are quite accurate for excited states of the $3s^23p^33d$ configuration.

The HFR results reported by Fawcett[27] agree with the present calculations with an average difference of 1.5%, and the maximum difference of 7.6% appears for the $^1D_2$ (level 4). Clearly, the level energies of Chou *et al.*[28] disagree with experimental values within 12%, and we did not provide a comparison with these previous MCDF results. When compared to superstructure (SS) calculations of Bhatia and Doschek,[29] our present energies for the $3s^23p^4$ and $3s3p^5$ configurations lie closer to the NIST values. These SS calculations[29] yields an average percentage difference of 3.4% with NIST as well as present energies and few energies differ up to 8.4% like for the $3s^23p^4\ {}^3P_1$ state. The present GRASP energies show good agreement with MCDF energies of Aggarwal *et al.*[31] within 2.0%. We include an extra configuration $3s^23p3d^3$ in our calculations which generates 110 fine-structure levels in comparison to the atomic model of Aggarwal *et al.*[31]

The MR–MP energies reported by Ishikawa[32] have excellent accuracy within 0.13% with NIST values. However, this study does not report atomic data for the forbidden lines. The diagnostics and interpretation of forbidden spectral lines among ground configuration levels highlight the need for accurate atomic data. A more detailed comparison of present energies with the MR–MP theory shows that our GRASP energies agree within 0.03%–2%, whereas FAC energies agree well in the range from 0.09% to 2.1%. For the $3s^23p^4$–$^1D_1$ level, we find a relatively large difference of 3.9% for GRASP and 3.4% for FAC. Overall, our calculated energies are seen to be in close agreement with MR–MP theory with an average difference of 0.05 Ryd.

The ordering of some energy levels are different among various calculations of Ni XIII. For most exchanged levels, the spectroscopic terms are different but the $2J$-values are the same. These quantities are used to match energy levels between different calculations. The ordering of 48 energy levels from GRASP and FAC is the same except for the 37/38 ($^3P_2/^1P_1$) and 48 ($3p^6\ {}^1S_0$) levels. The ordering of some energy levels 30/31 ($^3F_3/^3D_2$), 32/33 ($^3F_4/^3F_2$), and 37/38 ($^3P_2/^1P_1$) in our GRASP calculations do not correspond to the level ordering of GRASP calculations of Aggarwal *et al.*[31] due to differing amount of CI by the additional configuration $3s^23p3d^3$. In some cases both our calculations differ slightly with SS calculations. The level ordering produced using the MR–MP theory and our GRASP calculations are the same except the order of 31/33 ($^3D_2/^3F_2$) and 40/41($^3P_0/^3P_1$) levels due to closely related energies and difference of relativistic effects considered in the MR–MP and present MCDF methods. We note that our calculated energies are in much better agreement with the experimental values than the previous calculations[28,29,31] in particular for the $3s^23p^33d$ configuration levels.

3.2. Wavelengths, oscillator strengths, and transition rates

We have reported wavelengths (λ_{ji} in unit Å), transition rates (A_{ji} in unit s^{-1}), and oscillator strengths (f_{ji}) of E1, E2, and M1 transitions among the lowest-lying 48 levels of Ni XIII. The forbidden lines among the levels of the ground state configuration of S-like ions[40] are of interest for the astrophysical and tokamak plasma. However, there are significant differences among the available radiative data of Ni XIII. Therefore, we revisit and update these transition data so that these atomic parameters can be reliably used for diagnostics and modelling purposes.

In Table 2 we compare our calculated wavelengths, transition rates, and weighted oscillator strengths for E1 transitions from all 48 upper levels to the levels of ground state configuration. The E1 transition to other levels in Ni XIII do not exist. The level indices of lower and upper levels of transitions are defined in Table 1. For some weak transitions such as $3s3p^5\ {}^3P_1 \rightarrow 3s^23p^4\ {}^1S_0$, our calculated wavelengths differ within the 3-Å transition due to CI effects. For all other transitions, our computed wavelengths agree within the average percent difference of 0.08%. Overall, GRASP calculated wavelengths are higher than the FAC values for the majority of transitions. The A-values obtained from GRASP and FAC differ within 5% for most of the strong lines, whereas differences for a few weaker transitions vary from 15%–43% such as 17-3 ($3s^23p^33d\ {}^3D_1 \rightarrow 3s^23p^4\ {}^3P_0$).

Similarly, GRASP weighted oscillator strengths yield a maximum discrepancy of 41% with the corresponding FAC values. Our two calculations for gf-values agree within 5% for the majority of the transitions. In the last column of Table 2, we present the ratio of the length and velocity forms of the GRASP calculated oscillator strengths which provide an indication about their accuracy. This ratio of oscillator strengths is near unity (identical f-values) for most of the transitions with oscillator strengths (≥ 0.01) which clearly indicates the accuracy of the GRASP data. Table 2 clearly shows that radiative data for almost all strong transitions ($f \geq 0.01$) are accurate to better than 10%. However, for some weak transitions ($gf \leq 0.01$), both our calculations differ by a factor of 1.5 (43%) at most.

Table 2. Comparison of wavelengths λ (Å), transition rates A_{ij} (s^{-1}) and weighted oscillator strengths ($g_i f_{ji}$) in Ni XIII. The number form expression $a \pm b \equiv a \times 10^{\pm b}$.

Transition		λ_{ji}		A_{ji}		$g_i f_{ji}$		
j	i	GRASP	FAC	GRASP	FAC	GRASP	FAC	R
6	1	306.37	305.17	2.82 +09	2.92 +09	2.00 –1	2.04 –1	0.9
7	1	293.78	292.69	1.96 +09	2.03 +09	7.60 –2	7.83 –2	0.9
9	1	236.32	235.99	5.11 +08	5.18 +08	1.30 –2	1.30 –2	0.8
11	1	223.04	222.91	1.27 +08	1.31 +08	2.80 –3	2.93 –3	0.9
12	1	222.92	222.79	1.36 +08	1.39 +08	5.10 –3	5.18 –3	0.9
13	1	222.71	222.59	4.94 +07	5.03 +07	2.60 –3	2.62 –3	0.9
15	1	209.30	209.36	8.01 +07	8.22 +07	2.60 –3	2.70 –3	1.2
16	1	207.03	207.06	3.21 +6	3.04 +6	1.44 –4	1.37 –4	0.0
17	1	205.97	205.97	4.61 +07	3.04 +06	8.80 –4	8.96 –4	1.0
18	1	203.49	203.55	6.11 +07	4.70 +07	1.90 –3	1.98 –3	1.1
20	1	201.65	201.73	2.09 +07	6.36 +07	8.90 –4	9.07 –4	1.3
22	1	191.11	191.29	1.22 +08	2.12 +07	4.70 –3	4.85 –3	1.0
26	1	183.82	184.04	3.48 +08	3.55 +08	8.80 –3	9.02 –3	0.9
27	1	178.92	179.18	3.49 +08	3.55 +08	5.00 –3	5.13 –3	0.9
29	1	177.44	177.63	4.23 +09	4.31 +09	6.00 –2	6.12 –2	0.9
30	1	176.41	176.60	4.28 +08	4.40 +08	1.40 –2	1.44 –2	1.0
31	1	176.14	176.36	3.00 +07	4.01 +07	7.00 –4	9.36 –4	1.1
33	1	174.97	175.19	1.15 +09	1.18 +09	2.60 –2	2.72 –2	0.9
34	1	173.08	173.28	8.46 +09	8.71 +09	1.90 –1	1.96 –1	0.9
35	1	171.69	171.93	5.84 +08	6.04 +08	1.80 –2	1.87 –2	1.0
36	1	162.15	162.44	2.80 +09	2.87 +09	7.70 –2	7.96 –2	1.0
37	1	161.35	161.75	1.16 +11	1.14 +11	2.30 –0	2.24 –0	1.0
38	1	161.16	161.55	1.02 +11	1.01 +11	1.20 –0	1.18 –0	1.0
39	1	159.87	160.28	2.66 +10	2.60 +10	3.10 –1	3.00 –1	0.9
41	1	157.37	157.76	2.32 +09	2.17 +09	2.60 –2	2.43 –2	1.2
42	1	154.50	154.97	1.66 +11	1.62 +11	4.10 –0	4.08 –0	1.0
43	1	151.99	152.44	3.37 +10	3.29 +10	5.80 –1	5.73 –1	1.0
44	1	150.49	150.93	2.88 +09	2.80 +09	2.90 –2	2.87 –2	1.0
45	1	146.77	147.19	1.18 +08	1.13+08	1.90 –3	1.83 –3	0.7
46	1	143.44	143.92	5.18 +08	4.69 +08	1.10 –2	1.02 –2	1.1
47	1	136.91	137.43	4.37 +05	6.08+05	3.68 –6	5.16 –6	0.1
6	2	325.66	324.26	8.67 +08	8.97 +08	6.90 –2	7.07 –2	0.9
7	2	311.47	310.20	9.50 +08	9.84 +08	4.10 –2	4.26 –2	0.9
8	2	302.77	301.55	4.07 +09	4.21 +09	5.60 –2	5.74 –2	0.9
9	2	247.63	247.25	3.44 +07	3.65 +07	9.50 –4	1.00 –3	0.9
10	2	233.28	233.11	2.18 +08	2.25 +08	1.80 –3	1.83 –3	0.9
11	2	233.09	232.92	6.27 +07	6.39 +07	1.50 –3	1.56 –3	0.9
12	2	232.96	232.80	1.56 +05	1.78 +05	6.30 –6	7.23 –6	1.4
15	2	218.13	218.17	1.50 +07	1.47 +07	5.35 –4	5.25 –4	0.7
17	2	214.51	214.50	2.58 +07	2.71 +07	5.30 –4	5.60 –4	1.5
18	2	211.82	211.87	1.32 +06	1.42 +06	4.43 –5	4.78 –5	0.0
19	2	210.03	210.01	1.11 +08	1.14 +08	7.40 –4	7.51 –4	0.9
26	2	190.59	190.81	1.03 +08	1.04 +08	2.80 –3	2.83 –3	0.9
27	2	185.33	185.60	9.98 +07	1.00 +08	1.50 –3	1.55 –3	1.1
28	2	184.81	184.98	2.52 +08	2.42 +08	1.29 –3	1.24 –3	0.6
29	2	183.74	184.04	1.72 +04	1.17+05	2.61 –7	1.78 –6	28.4
31	2	182.35	182.57	2.18 +07	3.37 +07	5.40 –4	8.43 –4	1.3
33	2	181.10	181.32	2.46 +09	2.50 +09	6.00 –2	6.17 –2	1.0
34	2	179.07	179.27	1.73 +09	1.78 +09	4.20 –2	4.29 –2	0.9
37	2	166.54	166.96	2.22 +10	2.17 +10	4.60 –1	4.54 –1	1.0
38	2	166.35	166.75	4.73 +09	4.81 +09	5.90 –2	6.02 –2	1.1
39	2	164.97	165.40	2.54 +10	2.51 +10	3.10 –1	3.09 –1	0.9
40	2	162.39	162.80	1.59 +11	1.57 +11	6.30 –1	6.25 –1	1.0
41	2	162.31	162.71	4.57 +10	4.46 +10	5.40 –1	5.31 –1	1.0
43	2	156.60	157.06	1.23 +11	1.21 +11	2.30 –0	2.24 –0	1.0
44	2	155.00	155.46	6.92 +10	6.78 +10	7.50 –1	7.37 –1	1.0

Table 2. (continued)

Transition		λ_{ji}		A_{ji}		$g_i f_{ji}$		
j	i	GRASP	FAC	GRASP	FAC	GRASP	FAC	R
45	2	151.06	151.49	1.08 +10	1.07 +10	1.80 –1	1.84 –1	1.0
47	2	140.63	141.10	8.42 +08	8.34 +08	7.50 –3	7.47 –3	1.1
7	3	312.15	310.86	1.20 +09	1.24 +09	5.30 –2	5.39 –2	0.9
9	3	248.06	247.81	1.97 +05	2.05 +05	5.45 –6	5.65 –6	0.1
11	3	233.47	233.30	2.63 +07	2.72 +07	6.40 –4	6.67 –4	1.0
17	3	214.84	214.81	2.08 +05	1.46 +05	4.30 –6	3.03 –6	4.7
27	3	185.57	185.84	1.48 +09	1.51 +09	2.30 –2	2.35 –2	1.0
29	3	183.98	184.17	1.04 +08	1.05 +08	1.60 –3	1.60 –3	0.8
38	3	166.54	166.94	1.20 +10	1.20 +10	1.50 –1	1.51 –1	1.0
39	3	165.16	165.58	1.18 +10	1.17 +10	1.40 –1	1.45 –1	0.9
41	3	162.49	162.89	3.70 +10	3.61 +10	4.40 –1	4.31 –1	1.0
44	3	155.17	155.62	9.38 +10	9.18 +10	1.00 –0	9.99 –1	1.0
47	3	140.77	141.24	1.38 +09	1.32 +09	1.20 –2	1.19 –2	1.0
6	4	360.27	358.39	1.21 +08	1.25 +08	1.20 –2	1.21 –2	0.9
7	4	342.99	341.30	6.51 +06	6.85 +06	3.44 –4	3.59 –4	0.3
9	4	267.15	266.61	1.02 +10	1.04 +10	3.30 –1	3.32 –1	0.8
11	4	250.31	250.03	1.90 +06	2.19 +06	5.40 –5	6.16 –5	0.8
12	4	250.15	249.88	1.44 +06	1.46 +06	6.80 –5	6.82 –5	1.1
13	4	249.89	249.63	4.69 +05	4.78 +05	3.10 –5	3.13 –5	0.7
15	4	233.14	233.11	2.02 +07	2.10 +07	8.20 –4	8.54 –4	0.7
16	4	230.32	230.26	1.17 +06	1.15 +06	6.51 –5	6.39 –5	0.3
17	4	229.01	228.92	9.86 +05	1.01 +06	2.30 –5	2.38 –5	1.1
18	4	225.94	225.93	3.26 +05	2.97 +05	1.25 –5	1.14 –5	0.4
20	4	223.68	223.69	2.05 +07	2.09 +07	1.10 –3	1.10 –3	1.0
22	4	210.78	210.93	1.04 +08	1.05 +08	4.80 –3	4.91 –3	1.0
26	4	201.95	202.14	1.09 +09	1.10 +09	3.30 –2	3.36 –2	0.8
27	4	196.05	196.30	7.27 +08	7.46 +08	1.30 –2	1.29 –2	1.0
29	4	194.28	194.44	6.01 +08	6.24 +08	1.00 –2	1.06 –2	1.0
30	4	193.04	193.20	1.64 +08	1.67 +08	6.40 –3	6.55 –3	1.0
31	4	192.72	192.91	1.14 +08	1.09 +08	3.20 –3	3.05 –3	0.8
33	4	191.32	191.52	1.81 +08	1.88 +08	5.00 –3	5.18 –3	1.0
34	4	189.06	189.23	5.27 +08	5.42 +08	1.40 –2	1.46 –2	0.9
35	4	187.41	187.62	9.83 +07	1.01 +08	3.60 –3	3.74 –3	1.1
36	4	176.09	176.38	6.84 +07	6.99 +07	2.20 –3	2.28 –3	0.7
37	4	175.15	175.57	2.97 +09	2.92 +09	6.80 –2	6.75 –2	1.0
38	4	174.93	175.34	2.49 +10	2.43 +10	3.40 –1	3.36 –1	1.0
39	4	173.41	173.84	5.30 +10	5.23 +10	7.20 –1	7.11 –1	1.0
41	4	170.47	170.87	5.22 +10	5.23 +10	6.80 –1	6.87 –1	1.0
42	4	167.12	167.61	1.38 +08	1.20 +08	4.00 –3	3.55 –3	0.8
43	4	164.18	164.66	4.68 +09	4.66 +09	9.40 –2	9.46 –2	0.9
44	4	162.43	162.90	4.79 +08	4.78 +08	5.70 –3	5.70 –3	1.1
45	4	158.10	158.55	1.22 +11	1.20 +11	2.30 –0	2.26 –0	1.0
46	4	154.24	154.76	1.83 +11	1.79 +11	4.60 –0	4.49 –0	1.0
47	4	146.72	147.20	1.93 +09	1.93 +09	1.90 –2	1.88 –2	0.8
7	5	413.79	411.02	3.13 +07	3.24 +07	2.40 –3	2.46 –3	0.8
9	5	308.23	307.34	3.35 +08	3.48 +08	1.40 –2	1.48 –2	1.1
11	5	286.02	285.51	1.57 +05	1.40 +05	5.80 –6	5.12 –6	0.7
17	5	258.54	258.31	4.28 +06	4.34 +06	1.30 –4	1.30 –4	0.6
27	5	217.30	217.52	9.99 +07	1.03 +08	2.10 –3	2.19 –3	1.0
29	5	215.12	215.24	1.93 +06	1.61 +06	4.03 –5	3.35 –5	0.0
38	5	191.66	192.08	1.83 +09	1.81 +09	3.00 –2	3.00 –2	1.0
39	5	189.83	190.28	1.68 +09	1.68 +09	2.70 –2	2.74 –2	1.1
41	5	186.31	186.73	6.90 +09	6.94 +09	1.10 –1	1.09 –1	1.0
44	5	176.75	177.25	4.51 +07	3.90 +07	6.30 –4	5.51 –4	1.1
47	5	158.31	158.82	1.45 +11	1.42 +11	1.60 –0	1.61 –0	1.0

R: The ratio of velocity/length form of oscillator strengths from the GRASP calculations.

To further assess the accuracy of our results, we compare present oscillator strengths for some selected E1 transitions ($f \geq 10^{-3}$) with other theoretical oscillator strengths[27–29,31] in Table 3. For most of the strong transitions, both our FAC and GRASP oscillator strengths agree well within 10% with previous MCDF calculations.[31] For some weaker transitions ($f \leq 10^{-2}$), the significant differences from 50%–100% are found. However, our calculated oscillator strengths from GRASP and FAC perfectly agree for these transitions. The present oscillator strengths for the two weak transitions (39–3, 41–4) are consistent with MCDF values of Ref. [28]. Our FAC and GRASP oscillator strengths are relatively smaller than the previous GRASP[31] and superstructure calculations of Bhatia *et al.*[29] up to a factor of 3. There are considerable differences in f-values between the present and other calculations[27–29] due to strong level mixing and CI effects. Our present GRASP and previous GRASP[31] calculated f-values are in close agreement. The large differences ($\sim 50\%$) are associated with weaker transitions.

Table 3. Comparison of oscillator strengths f_{ji} for E1 transitions with other calculations. The number form expression $a \pm b \equiv a \times 10^{\pm b}$.

j	i	GRASP	FAC	MCDF[a]	MCDF[b]	SS	GRASP
6	1	3.97 –2	4.08 –2	3.54 –2	4.57 –2	4.80 –2	4.42 –2
7	1	1.52 –2	1.57 –2	1.36 –2	1.75 –2	1.79 –2	1.70 –2
29	1	1.20 –2	1.22 –2	8.60 –3	6.31 –3	1.16 –2	6.08 –3
34	1	3.80 –2	3.92 –2	2.48 –2	1.81 –2	1.72 –2	1.79 –2
37	1	2.38 –1	2.36 –1	3.37 –1	5.67 –3	1.75 –1	1.31 –1
38	1	4.54 –1	4.48 –1	5.18 –1	1.20 –1	7.13 –1	4.71 –1
39	1	6.13 –2	6.00 –2	1.48 –1	1.39 –1	1.99 –1	1.76 –1
42	1	8.30 –1	8.16 –1	9.38 –1	8.35 –1	1.09 –0	8.47 –1
43	1	1.17 –1	1.15 –1	1.25 –1	4.61 –1	1.08 –1	1.22 –1
44	1	5.86 –3	5.73 –3	6.02 –3	6.16 –3	5.94 –3	5.93 –3
6	2	2.30 –2	2.36 –2	2.10 –2	2.64 –2	2.84 –2	2.54 –2
7	2	1.38 –2	1.42 –2	1.27 –2	1.59 –2	1.67 –2	1.53 –2
8	2	1.86 –2	1.91 –2	1.67 –2	2.17 –2	2.23 –2	2.07 –2
34	2	1.39 –2	1.43 –2	1.03 –2	7.38 –3	1.21 –2	7.17 –3
38	2	1.54 –1	1.51 –1	1.59 –1	7.55 –1	1.98 –1	1.70 –1
40	2	2.10 –1	2.08 –1	2.25 –1	3.04 –2	3.00 –1	2.09 –1
41	2	1.80 –1	1.77 –1	1.97 –1	6.68 –4	5.77 –2	2.73 –1
43	2	7.57 –1	7.45 –1	8.43 –1	1.63 –1	9.93 –1	7.64 –1
44	2	2.49 –1	2.46 –1	2.76 –1	2.71 –1	3.14 –1	2.48 –1
45	2	6.16 –2	6.12 –2	8.37 –2	5.04 –2	1.22 –1	5.05 –2
27	3	2.30 –2	2.35 –2	3.00 –2	2.76 –2	2.16 –2	2.65 –2
39	3	1.45 –1	1.45 –1	2.72 –1	1.60 –1	6.91 –2	1.06 –2
41	3	4.40 –1	4.31 –1	5.14 –1	1.22 –2	3.20 –1	5.47 –1
44	3	1.00 –0	9.99 –1	1.15 –0	5.37 –1	1.32 –0	1.02 –0
9	4	6.53 –2	6.64 –2	5.90 –2	1.87 –5	6.84 –2	6.87 –2
37	4	6.84 –2	6.71 –2	2.62 –2	8.25 –4	1.03 –1	1.77 –1
39	4	1.43 –1	1.42 –1	2.01 –1	1.61 –1	6.43 –3	1.38 –1
41	4	1.37 –1	1.37 –1	1.40 –1	1.40 –1	4.03 –1	2.84 –2
45	4	4.58 –1	4.51 –1	5.60 –1	4.64 –1	5.13 –1	4.68 –1
46	4	9.12 –1	8.98 –1	9.12 –1	8.98 –1	1.24 –0	9.20 –1
9	5	1.43 –2	1.48 –2	–	2.33 –6	4.61 –3	1.94 –2
38	5	3.02 –2	3.00 –2	2.00 –2	6.43 –2	4.38 –4	6.50 –2
41	5	1.10 –1	1.09 –1	8.60 –2	4.91 –2	1.00 –1	5.55 –2
47	5	1.63 –0	1.61 –0	1.97 –0	1.61 –0	2.12 –0	1.64 –0

[a]MCDF calculations of Fawcett;[27] [b]MCDF calculations of Chou *et al.*;[28] SS: Superstructure calculations of Bhatia and Doschek;[29] GRASP: Calculations of Aggarwal *et al.*[31]

In Table 4 we compare our computed wavelengths with measured wavelengths[16,36] and MCDF calculations of Aggarwal *et al.*[31] Shirai *et al.*[36] have critically analyzed and compiled the energy levels, wavelength, oscillator strengths, and transition probabilities for allowed as well as forbidden transitions in Ni XI–Ni XXVII. In addition, measured wavelengths of highly charged Ni ions from 120 Å–400 Å with beam-foil spectroscopy have been reported by Yang *et al.*[16] Since these two experimentally measured wavelengths ($3s3p^5\ ^1P_1 \rightarrow 3s^23p^4\ ^3P_1$) differ by 5.7 Å. The theoretical wavelengths for the transitions ($3s^23p^3 3d \rightarrow 3s^23p^4\ ^3P_{2,1,0},\ ^1D_2$) calculated by Aggarwal *et al.*[31] show significant differences within 7.4 Å (4.8%) with those of measured wavelengths.[16,36]

Table 4. Comparison of wavelengths λ_{ji} (Å) of some E1 transitions in Ni XIII.

Transitions		Present		Previous		
j	i	GRASP	FAC	SRD	Theory	Expt.
6	1	306.37	305.17	302.84	303.58	
6	2	325.66	324.26	321.88	322.21	
7	1	293.78	292.69	290.57	291.15	
7	2	311.47	310.20	308.05	308.52	
7	3	312.15	310.86	308.54	309.19	
9	4	267.15	266.61	267.47	264.62	
37	1	161.35	161.75	164.17	159.77	
37	2	166.54	166.94	169.61	164.87	163.96
42	1	154.50	154.97	157.73	151.30	157.71
43	1	151.99	152.44	155.12	148.71	
43	2	156.60	157.06	159.97	153.12	159.94
44	3	155.17	155.62	158.77	151.68	
45	2	151.06	151.49	154.68	147.30	
45	4	158.10	158.55	161.55	153.99	
46	4	154.24	154.76	157.53	150.70	

SRD: Experimental wavelength data compiled by Shirai *et al.*;[36] Theory: GRASP calculations of Aggarwal *et al.*;[31] Expt.: Experimental measurements by Yang *et al.*[16]

The accuracy of present FAC computed wavelengths varies within 0.9 Å–3.2 Å with the experimental measurements. Our FAC wavelengths are 0.4 Å–1.3 Å higher than MCDF[31] values and lie closer to the experimental results for ($3s^23p^3 3d$) decays. On the other hand, the MCDF predicted transition wavelength among the lowest lying levels associated with the Ni XIII ground and $3s3p^5$ configurations agree well within 0.7 Å with experimental values.[36] Our GRASP calculated wavelength for the 9–4 ($3s3p^5\ ^1P_1 \rightarrow 3s^23p^4\ ^1D_2$) transition at $\lambda = 267.15$ Å show excellent agreement (0.3 Å) with the observed wavelength[36] at $\lambda = 267.47$ Å, while the FAC value is smaller by 0.9 Å. The discrepancies between the present GRASP calculated wavelengths of Ni XIII and measured ones are on the order of 3.2 Å or 2.0% calculations.

In Table 5 we report wavelengths, oscillator strengths and transition rates for magnetic dipole M1 transitions between the

$3s^23p^4$ and $3s3p^5$ levels in length form. In this table we also include the available experimental[36] and other theoretical[33,41] transition data. For M1 transitions, our present calculated wavelengths show reasonable agreement with experimental values[36] within 78 Å. However, the wavelength data provided by the HFR[41] and multi-configuration Dirac–Hartree–Fock (MCDHF) calculations[33] are of higher accuracy than the present results except 3–2 transition.

The present calculations for transition rates of M1 transitions show good agreement with HFR[41] and MCDHF calculations[33] within 15% except 3–2 transition where the maximum difference is 131%. This is expected in weaker transitions of the M1 type where the uncertainties are often larger. Since the M1 transition rates are proportional to the $(\Delta E)^3$ transition wavelength, thus, an error in wavelength (transition energy) is typically dominated in transition rates. Furthermore, f-values obtained from GRASP and FAC show good agreement with each other for all M1 transitions but they markedly disagree with MCDHF calculations. The largest difference of 400% appears for the 2–1 forbidden transition.

Table 5. Comparison of wavelengths λ_{ji} (in unit Å), oscillator strengths (f_{ji}), and transition rates A_{ji} (in unit s^{-1}) of magnetic dipole M1 transitions in Ni XIII. The number form expression $a \pm b \equiv a \times 10^{\pm b}$.

Transitions		λ_{ji}			f_{ji}			A_{ji}			
j	i	GRASP	FAC	Others	GRASP	FAC	DHF[c]	GRASP	FAC	HFR[b]	DHF[c]
2	1	5171.13	5182.95	5115.80[a] 5117.24[c] 5116.50[b]	1.8 –6	1.83 –6	3.696 –7	1.53 +2	1.52 +2	1.574 +2	1.569 +2
4	1	2047.48	2054.91	2125.50[a] 2126.17[c] 2125.40[b]	8.3 –7	8.26 –7	1.699 –7	2.63 +2	2.61 +2	2.590 +2	2.507 +2
3	2	143056.01	145979.50	192975.75[c] 166068[b]	5.1 –8	5.01 –8	1.260 –8	1.67 –2	1.57 –2	1.069 –2	6.770 –3
4	2	3389.56	3404.85	3637.54[c] 3635.60[b]	1.8 –7	1.78 –7	5.927 –8	2.07 +1	2.05 +1	1.845 +1	1.793 +1
5	2	1259.68	1264.66	1277.23[a] 1277.23[c] 1277.10[b]	6.1 –7	6.06 –7	2.042 –7	2.55 +03	2.53 +3	2.55 +03	2.50 +03
7	6	7149.53	7154.58		1.4 –6	1.39 –6		6.05 +1	6.03 +1		
9	6	1033.56	1041.07		1.6 –7	1.63 –7		3.35 +2	3.35 +2		
8	7	10832.79	10805.25		7.3 –7	7.36 –7		4.18 +1	4.21 +1		
9	7	1208.22	1218.35		8.2 –8	8.25 –8		1.25 +2	1.24 +2		
9	8	1359.89	1373.18		9.8 –8	9.94 –8		1.18 +2	1.17 +2		

[a]Experimental wavelength data compiled by Shirai *et al.*;[36] [b]HFR calculations by Biémont and Hansen;[41] [c]MCDHF calculations of Froese Fischer.[33]

Table 6. Comparison of wavelengths λ_{ji} (in unit Å), oscillator strengths (f_{ji}), and transition rates A_{ji} (in unit s^{-1}) of electric-quadrupole E2 transitions in Ni XIII. The number form expression $a \pm b \equiv a \times 10^{\pm b}$.

Transitions		λ_{ji}			f_{ji}			A_{ji}			
j	i	GRASP	FAC	DHF[b]	GRASP	FAC	DHF[b]	GRASP	FAC	HFR[a]	DHF[b]
2	1	5171.13	5182.95	5117.24	2.19 –10	4.39 –11	4.47 –11	1.82 –2	1.82 –2	1.92 –2	1.90 –2
3	1	4990.73	5005.24	4985.04	2.45 –14	2.68 –11	2.70 –11	6.55 –6	3.57 –2	3.70 –2	3.62 –2
4	1	2047.48	2054.91	2126.17	1.47 –09	2.90 –10	2.76 –10	4.68 –1	4.58 –1	4.25 –1	4.07 –1
5	1	1012.93	1016.60	1022.12	5.83 –09	7.52 –11	8.89 –11	3.79 +1	2.43 +0	2.73 +0	2.84 +0
4	2	3389.56	3404.85	3637.54	4.87 –11	1.69 –11	1.46 –11	5.65 –3	5.84 –3	4.45 –3	4.41 –3
4	3	3471.82	3486.16	3707	1.20 –12	4.47 –11	3.71 –11	1.34 –4	4.91 –3	3.44 –3	3.60 –3
5	4	2004.70	2011.95	1968.38	4.44 –09	1.27 –09	1.35 –09	7.38 –0	1.04 +1	1.16 +1	1.17 +1
7	6	7149.53	7154.58		6.87 –11	1.49 –11		2.99 –3	3.23 –3		
8	6	4306.97	4304.44		1.58 –10	3.07 –11		5.69 –2	5.53 –2		
9	6	1033.56	1041.07		1.22 –09	9.46 –11		2.53 –0	9.71 –1		
9	7	1208.22	1218.35		5.66 –10	2.76 –10		8.62 –1	1.24 +0		

[a]HFR calculations by Biémont and Hansen;[41] [b]MCDHF calculations of Froese Fischer.[33]

Comparison of selected wavelengths, oscillator strengths and transition rates for electric quadrupole E2 transitions among the lowest lying 9 states of Ni XIII is given in Table 6. Our GRASP and FAC calculated wavelengths exhibit good agreement within 15 Å with each other. The maximum difference of FAC predictions with MCDHF wavelengths are up to an order of 232 Å at $\lambda = 3404.85$ Å 4–2 transition. The present GRASP value shows an uncertainty of 247 Å for the

same E2 transition. Overall, present calculated wavelengths for E2 transitions agree well with each other as they include more electron correlation effects than the previous MCDHF calculations. All the present FAC transition rates for E2 transitions listed in Table 6 show good agreement with HFR and MCDHF results[33,41] within 10% except for the two transition (4–2, 4–3) where the maximum difference is 42%. There is satisfactory agreement for E2 transition rates in the present calculations.

Similarly, our FAC f-values for the E2 transition in Ni XIII agree very well within 20% with those of MCDHF calculations, but differ substantially with the present GRASP values up to a factor of 12. The maximum difference of the order of 77 appears for 5–1 transition. Finally, we conclude that weaker transitions (M1 and E2) are more susceptible due to varying amount of CI effects, and thus such large differences in transition parameters are very common. This detailed comparison reflects that our results from the FAC are expected to be accurate to 10% for most of the strong transitions. Therefore, we believe that our calculated M1 and E2 transition data will be helpful in spectral analysis in astrophysics and fusion plasma research.

3.3. Radiative lifetimes

Radiative lifetime τ of an excited level j is obtained from the following expression

$$\tau_j = \frac{1}{\sum_i A_{ji}}. \quad (4)$$

Our calculated radiative lifetimes of 48 excited levels of Ni XIII in length form using the GRASP and FAC codes are listed in Table 1. This gauge of lifetimes appears to be more stable in the sense that it converges smoothly. Our calculated transition rates of the four types of transitions (E1, E2, M1, M2) obtained from FAC are used to obtain FAC lifetimes. The GRASP2 calculated lifetimes do not include the contributions from M2 transitions. All 48 lifetimes presented in Table 1 are in close agreement with each other within 11%. Träbert *et al.*[42–44] measured lifetimes for two levels of ground configuration $3s^2 3p^4$ ($^3P_1$, $^1D_2$) of Ni XIII measured with a heavy ion storage ring.

In Table 7, our present lifetimes of the levels of ground configuration are compared with experimental and previous theoretical results. For the $^3P_1$ state, both our calculated values are larger than the measured value[45] by 0.05 ms and 0.09 ms, respectively. Our present lifetimes for this state are in better agreement with the experimental lifetime than the previous theoretical values,[41,44,46] though the agreement of the previous MCDF value[28] is excellent for this state. We have derived the lifetime for the $^3P_0$ state from transition rates reported in Refs. [28] and [29]. Our present FAC lifetimes agree well within 0.1 ms with the calculations of Bhatia and Doschek.[29] For the same level, our GRASP value differs by almost a factor of 1.2 with MCDF results[28] because of the most important CI effects in both models.

Table 7. Comparison of lifetimes (millisecond-ms) of the ground configuration $3s^2 3p^4$ levels of Ni XIII with experimental and other theoretical results.

	Present		Others	
Term	GRASP	FAC	Theory	Expt.
$^3P_1$	6.55	6.59	6.37 [a]	6.50 ± 0.15 [l]
			6.35 [b]	
			6.51 [c]	
			6.35 [e]	
$^3P_0$	1.92 +4	1.95 +4	2.10 +4 [s]	
			1.59 +4 [c]	
$^1D_2$	3.51	3.55	3.62 [a]	4.50 ±0.20 [m]
			3.60 [b]	4.06 ±0.12 [n]
			3.67 [c]	
			3.99 [e]	
			3.72 [d]	
$^1S_0$	0.39	0.39	0.39 [a]	
			0.39 [b]	
			0.49 [c]	
			0.41 [e]	

[a]Calculations of Kaufman *et al.*;[46] [b]HFR calculations by Biémont and Hansen;[41] [c]MCDF calculations by Chou *et al.*;[28] [s]Superstructure calculations of Bhatia and Doschek;[29] [d]MCDF calculations by Froese Fischer;[33] [e]MR–MP calculations by Träbert *et al.*;[44] [l]Experimental measurements by Träbert *et al.*;[45] [m]Experimental measurements by Träbert *et al.*; [42] [n]Experimental measurements by Träbert *et al.*[43]

For the $^1D_2$ level, Träbert *et al.*[42,43] reported two experimental values which differ in magnitude by 0.4 ms. For this state, our present and other theoretical results are smaller than the experimental values by 22.0% at maximum. This significant discrepancy between theoretical and experimental results can be explained by the occurrence of cascades from 3d levels.[44] Also, for the $^1S_0$ state, our calculated lifetimes show good agreement with other theoretical results[41,46] and MR–MP calculations by Träbert *et al.*[44] However, we find that the present lifetimes for the $^1S_0$ level differ with MCDF[28] within 0.1 ms. Overall, our GRASP and FAC lifetimes agree well with other theoretical and experimental data for ground configuration levels lifetimes. We can therefore conclude that the configuration interaction model for NI XIII should form a good basis for calculating spectroscopic data.

3.4. Photoionization cross sections of Ni XII

In this work, we carried out calculations of PI cross sections for the ground and thirteen selected excited states of Ni XII using the fully relativistic Dirac R-matrix code. The target wavefunctions are obtained from the multi-configurational Dirac–Fock (MCDF)code GRASP code by using the EAL optimizing process for the concerned energy levels as described

above. We have selected a suitable energy step of 0.5 meV to envelop all thresholds in the target Ni XIII ion. The PI cross sections are calculated from their respective thresholds to well above the threshold of the last level to entail all thresholds in the target Ni XIII ion.

Table 8. Comparison of the present ionization energies (in unit eV) of Ni XII with NIST observed energies.

Levels	Terms	Present	NIST	% Err
$3s^23p^5$	$^2P^o_{3/2}$	351.988	351.63	0.10
···	$^2P^o_{1/2}$	348.950	348.700	0.07
$3s3p^6$	$^2S_{1/2}$	309.567	309.647	0.03
$3s3p^53d$	$^4P^o_{3/2}$	254.581		
···	$^4F^o_{3/2}$	248.846		
···	$^4D^o_{3/2}$	245.367		
···	$^2D^o_{3/2}$	242.911		
···	$^4P^o_{1/2}$	255.085		
···	$^4D^o_{1/2}$	245.567		
···	$^2P^o_{1/2}$	241.118		
$3s^23p^43d$	$^4D_{1/2}$	295.090		
···	$^2P_{1/2}$	291.056		
···	$^4P_{1/2}$	288.916		
···	$^2S_{1/2}$	272.652		
···	$^2P_{1/2}$	268.951	270.136	0.44

In Table 8, we compare our present calculated ionization threshold energies of Ni XII levels with the available NIST energies. Our MCDF calculated ionization energies are in excellent agreement with the NIST experimental values which ensures the accuracy of the present PI cross sections.

In Fig. 1, we show the total PI cross sections for the ground state configuration $3s^23p^5$ levels of Ni XII in length and velocity gauges. This ground state configuration generates two fine slitted levels ($^2P^o_{3/2}$, $^2P^o_{1/2}$). Our present length and velocity gauge PI cross sections for the ground state agree well within 9%. Since the length gauge is considered to be more stable and reliable than the velocity gauge, therefore, we plotted here length gauge PI cross sections for further discussions.

In Fig. 1(a), the threshold energy positions of core ion Ni XIII are labeled by small arrows. Figure 1(b) represents the PI cross section for the 1st metalstable state ($^2P^o_{1/2}$) in length form. In our calculations we find the strong resonances due to photoexcitation within the core states that enhance the cross sections by orders of magnitude. The resonance structures at some energy points owing to different Rydberg series are very narrow and unresolved due to very small energy differences between the energy levels of core ion as evident from Fig. 1(a). These resonances are less prominent between the 5th and 6th target states as there exists a discernible energy jump which causes less resonance structures in this energy span.

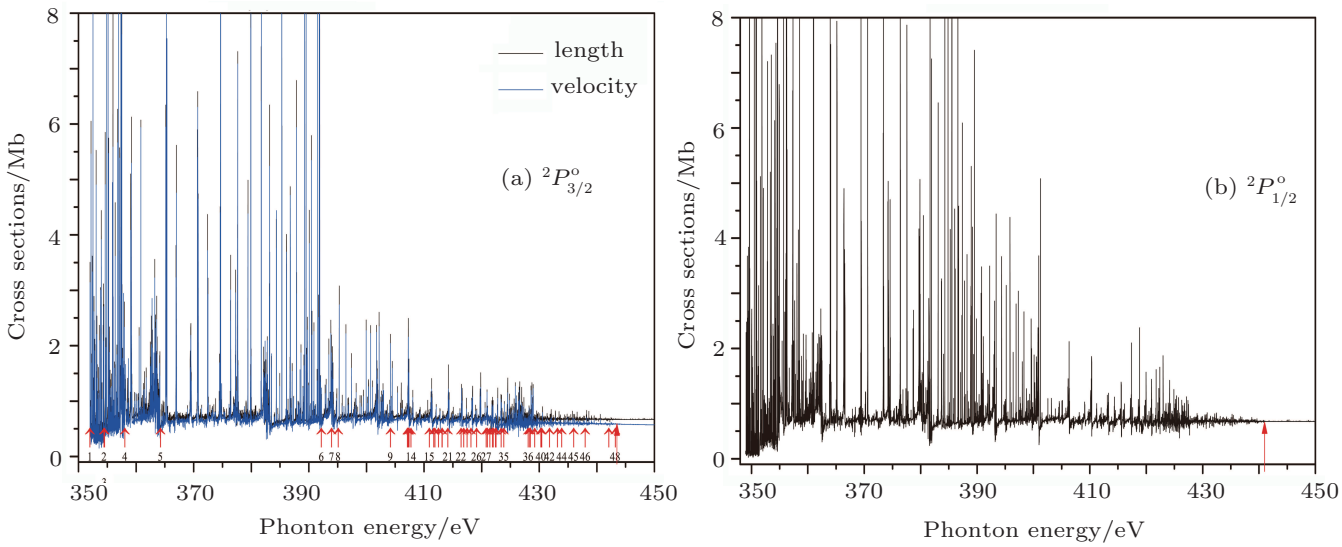


Fig. 1. (color online) Total PI cross sections of two levels from $3s^23p^5$ ($^2P^o_{3/2}$, $^2P^o_{1/2}$) of Ni XII. The excitation threshold positions are labeled according to Table 1. (a) Comparison of total PI cross sections in length and velocity forms for the ground state $^2P^o_{3/2}$, (b) total PI cross sections of the first metastable state $^2P^o_{1/2}$.

Figure 2 presents the comparison of our calculations for the mixture of ground state fine structure levels $^2P^o_{3/2}$, $^1P^o_{1/2}$ with the central field theoretical calculations.[38] For this comparison, we adopt the weighted average of two levels ($^2P^o_{3/2}$ and $^2P^o_{1/2}$) cross-sections using 2/3 and 1/2 as statistical weights for these two levels, respectively. There is a very good agreement between our R-matrix calculations and Verner[38] calculations for background contributions to PI cross sections at all energies as Verner's fit data lack of resonance profile. The data of Verner[38] exhibits a sharp ionization jump at $\sim$ 392 eV corresponding to the 3s threshold. This feature can also be observed in all PI profiles plotted in Figs. 1–5. To the best of our knowledge, no other theoretical or experimental data is available to compare the present results of PI cross

sections calculations.

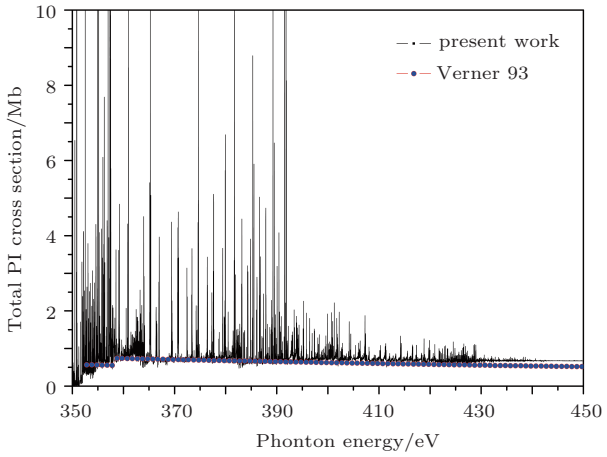


Fig. 2. Comparison between present DARC total PI cross sections in the ground state configuration $3s^23p^5$ ($^2P^o_{3/2}$, $^2P^o_{1/2}$) of Ni XII and previous theoretical calculations.[38]

Finally, we investigate the PI cross sections of some selected excited states of Ni XII. In Fig. 3 we show the total PI cross section for the metastable state $3s3p^6$ ($^2S_{1/2}$) of Ni XII. We find extensive resonances in the low energy region. The arrows in these panels point to the threshold energies corresponding to the last level of the target. Figure 4 represents total PI cross sections for five excited states ($^4D_{1/2}$, $^4P_{1/2}$, $^2P_{1/2}$, $^2P_{1/2}$, $^2S_{1/2}$) belonging to the $3s^23p^43d$ configuration of Ni XII. Figures 4(c) and 4(d) represent PI cross sections of two separate ($^2P_{1/2}$) states arising from $3s^23p^4$ (^1D) 3d and $3s^23p^4$ (^3P) 3d levels, respectively. All the five states show extensive resonances in the low energy region which enhance the PI cross sections in these energy regions.

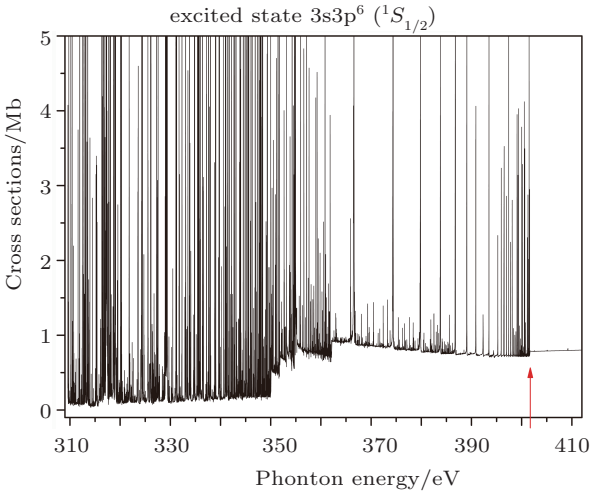


Fig. 3. (color online) Total PI cross sections of $3s3p^6$ ($^2S_{1/2}$) metastable state.

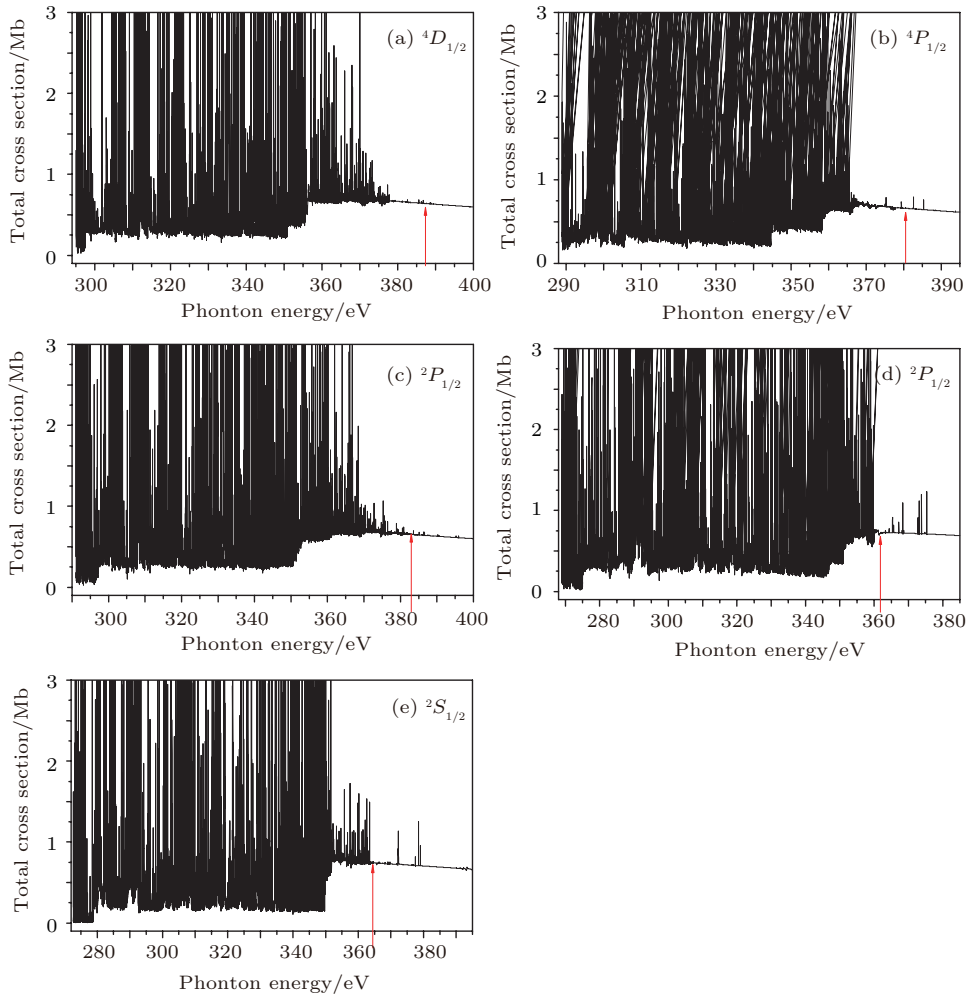


Fig. 4. (color online) Total PI cross sections in the excited state configuration $3s^23p^43d$ levels ($^4D_{1/2}$, $^4P_{1/2}$, $^2P_{1/2}$, $^2P_{1/2}$, and $^2S_{1/2}$).

Figure 5 illustrates total PI cross sections of $3s3p^5 3d$ six excited states ($^4P^o_{3/2,1/2}$, $^4D^o_{3/2,1/2}$, $^2P_{1/2}$, $^2D^o_{3/2}$). All these states contain same giant resonance structures owing to different Rydberg series of resonances converging at various thresholds from involved target states. Unfortunately, there are no other Ni XII PI cross sections available for comparison of these excited states.

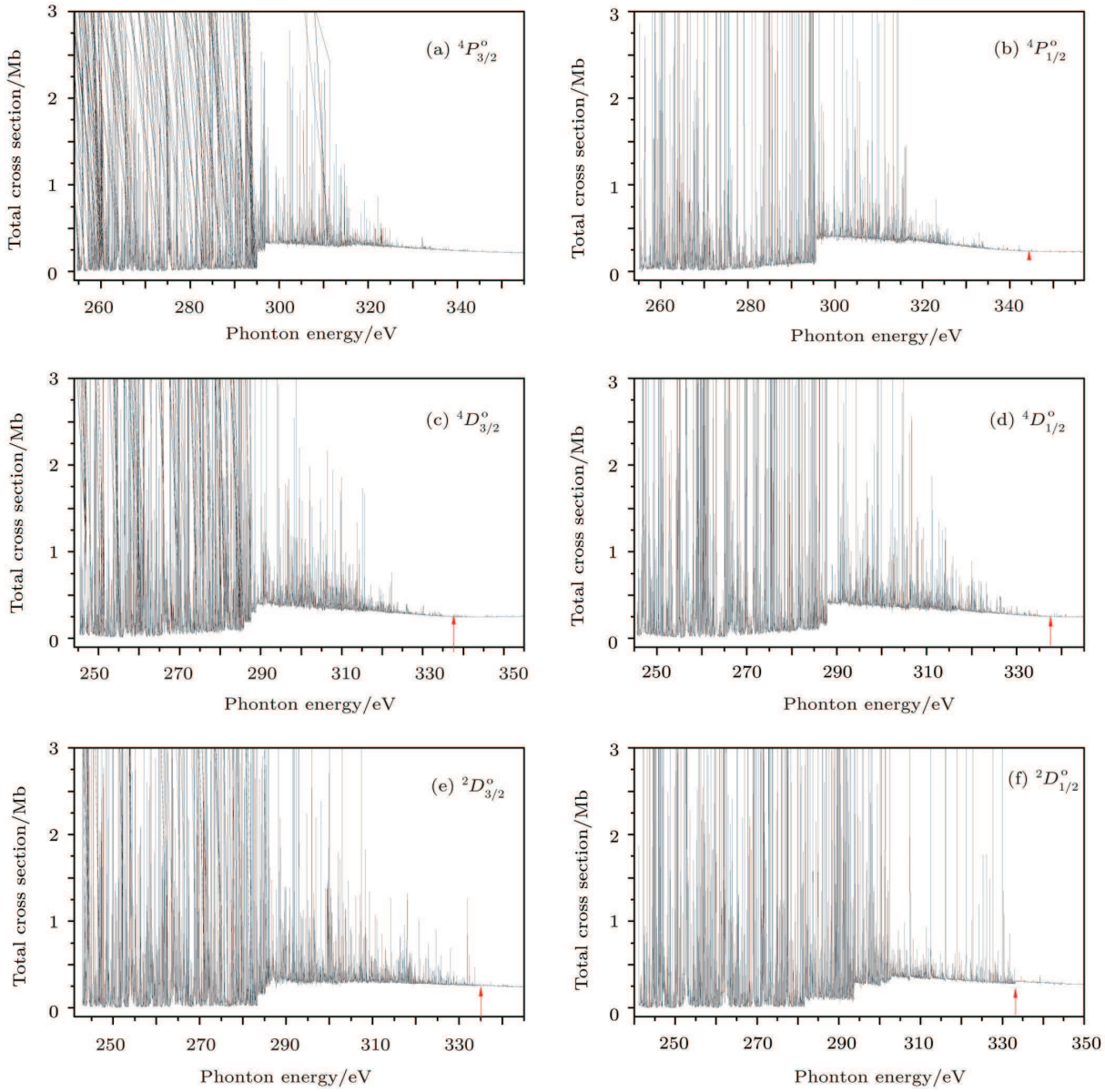


Fig. 5. (color online) Total PI cross sections in $3s3p^5 3d$ excited state configuration levels ($^4P^o_{3/2,1/2}$, $^4D^o_{3/2,1/2}$, $^2P^o_{1/2}$, and $^2D^o_{3/2}$).

4. Conclusions

In this paper, we have calculated fine-structure energy levels, wavelengths, oscillator strengths, transition rates, and radiative lifetimes for the lowest-lying 48 levels belonging to the $3s^2 3p^4$, $3s3p^5$, $3s^2 3p^3 3d$, and $3p^6$ configurations using two sets of fully relativistic GRASP and FAC codes. In the present work, we have included CI among the thirteen configurations ($3s^2 3p^4$, $3s3p^5$, $3p^6$, $3s^2 3p^3 3d$, $3s3p^3 3d^2$, $3p^5 3d$, $3s^2 3p3d^3$, $3s^2 3p^2 3d^2$, $3s3p^4 3d$, and $3s^2 3p^3 4l$, where l = s, p, d, and f). We present transition wavelengths, oscillator strengths, and transition rates of E1, E2, and M1 transitions. The relativistic corrections and QED effects have been included in our calculations. This represents a considerable extension of the available atomic structure data of Ni XIII. Our results of atomic structure parameters are in much better agreement with the available experimental and theoretical results.

Our results of energy levels associated with the $3s^2 3p^3 3d$ configuration agree closely with the NIST database within 2.0% and are found to be in good agreement with more accurate MR–MP theory values within the margin of the same accuracy (2.0%). Our FAC calculations provide more accurate results than our GRASP calculations owing to a different amount of CI, which is important for S-like systems. The accuracy of present radiative transition rates and absorption os-

cillator strengths are within 10% for most of the strong E1 transitions. The uncertainty in the oscillator strengths and transition rates of M1 and E2 transitions does not exceed 20% with the exception of a few transitions. It has been shown that radiative lifetimes obtained from the two sets are in good agreement with experimental and theoretical values.

Finally, we have reported the PI cross sections of some selected levels of Ni XII. We have used the fully relativistic R-matrix code DARC to calculate the PI cross-sections. Our results of total PI cross sections of ground state configuration levels are in good agreement with previous central field type data. In conclusion, our new reported data of Ni XIII are more extensive and accurate than the existing calculations. Our new calculated PI cross sections of Ni XII are useful for calculating radiative properties of nickel for astrophysical plasmas under the Opacity Project. The complete set of the present PI cross sections of Ni XII is available electronically.

References

[1] Bizau J M, Champeaux J P, Cubaynes D, Wuilleumier F J, Folkmann F, Jacobsen T S, Penent F, Blancard C and Kjeldsen H 2005 *Astron. Astrophys.* **439** 387

[2] Jerkstrand A, Fransson C, Maguire K, Smartt S, Ergon M and Spyromilio J 2012 *Astron. Astrophys.* **546** A28

[3] Pradhan A K and Nahar S N 2011 *Atomic Astrophysics and Astronomy* (Cambridge: Cambridge University Press)

[4] Cunto W, Mendoza C, Ochsenbein F and Zeippen C J 1993 *Astron. Astrophys.* **275** L5

[5] Del Zanna G and N R Badnell 2016 *Astron. Astrophys* **585** A118

[6] Miller J M, Raymond J, Fabian A, Steeghs D, Homan J, Reynolds C, van der Klis M and Wijnands R 2006 *Nature* **441** 953

[7] Kallman T R, Bautista M A, Goriely S, Mendoza C, Miller J M, Palmeri P, Quinet P and Raymond J 2009 *Astrophys. J.* **701** 865

[8] Tumra Tumra T, *et al.* 2009 *Astrophys. J.* **705** L62

[9] Tamagawa T 2010 *The* 10*th International Symposium on Origin of Matter and Evolution of Galaxies*, *AIP Conf. Proc.*, eds. Tanihara I *et al.*, Vol. 1269 (New York: Am. Inst. Phys.) p. 137

[10] Koyama K 2011 *The Galactic Center: A Window to the Nuclear Environment of Disk Galaxies.*, *ASP Conf. Ser.*, eds. Morris M R, Wang Q D and Yuan F, Vol. 439 (San Francisco: Astron. Soc. Pac.) p. 418

[11] Gabriel A H, Fawcett B C and Jordan C 1966 *Proc. Phys. Soc.* **87** 825

[12] Edlen B and Smitt R 1978 *Sol. Phys.* **57** 329

[13] Malinovsky L and Heroux M 1973 *Astrophys. J.* **181** 1009

[14] Raassen A J J, Mewe R, Audard M, Güel M, Behar E, Kaastra J S, van der Meer R L J, Foley C R and Ness J U 2002 *Astron. Astrophys* **389** 228

[15] Mattioli M, Fournier K B, Coffey I, Finkenthal M, Jupén C, Valisa M and Contributors to the EFDA-JET Work Programme 2004 *J. Phys. B: At. Mol. Opt. Phys.* **37** 13

[16] Yang Z H, Du S B, Zeng X T, Su H, Wang Y D and Zhang Y P 2005 *Chin. Phys.* **14** 953

[17] Kimura K, Yamazaki T and Achiba Y 1978 *Chem. Phys. Lett.* **58** 104

[18] Ruscic B and Berkowitz J 1983 *Phys. Rev. Lett.* **50** 675

[19] Hansen J E, Cowan R D, Carter S L and Kelly H P 1984 *Phys. Rev. A* **30** 1540

[20] van der Meulen P, Krause M O, Caldwell C D, Whitfield S B and de Lange C A 1992 *Phys. Rev. A* **46** 2468

[21] Krause M O, Caldwell C D, Whitfield S B, de Lange C A and van der Meulen P 1993 *Phys. Rev. A* **47** 3015

[22] Covington A M, Aguilar A, Alvarez I, *et al.* 2001 in *Proceedings of the XXII International Conference on Photonic, Electronic, and Atomic Collisions*, eds. Datz S, Bannister M E, Krause H F, Saddiq L H, Schultz D R and Vane C R (Princeton: Rinton Press) p. 48

[23] Alna'washi G A, Lu M, Habibi M, Phaneuf R A 2010 *Phys. Rev. A* **81** 053416

[24] Tyndall N B, Ramsbottom C A, Ballance C P and Hibbert A 2016 *MNRAS* **456** 366

[25] Dyall K G, Grant I P, Johnson C T and Plummer E P 1989 *Comput. Phys. Commun.* **55** 425

[26] Gu M F 2003 *Astrophys. J.* **582** 1241

[27] Fawcett B C 1986 *At. Data Nucl. Data Tables* **35** 185

[28] Chou H S, Chang J Y, Chang Y H and Huang K N 1996 *At. Data Nucl. Data Tables* **62** 77

[29] Bhatia A K and Doschek G A 1998 *At. Data Nucl. Data Tables* **68** 49

[30] Eissner W, Jones M and Nussbaumer H 1974 *Comput. Phys. Commun.* **8** 270

[31] Aggarwal K M, Keenan F P and Msezane A Z 2003 *At. Data Nucl. Data Tables***85** 453

[32] Ishikawa Y and Vilkas M J 2008 *Phys. Rev. A* **78** 042501

[33] Froese Fischer C 2010 *J. Phys. B: At. Mol. Opt. Phys.* **43** 074020

[34] Grant I P 2007 *Relativistic Quantum Theory of Atoms and Molecules* (Berlin: Springer)

[35] Jänsson P, Heb X, Froese Fischerb C and Grantc I P 2007 *Comput. Phys. Commun.* **177** 597

[36] Shirai T, Sugar J, Musgrove A and Wiese W L 2000 *J. Phys. C. Ref. Data* **8** 360

[37] Norrington P H 2004 www.am.qub.ac.uk/DARC

[38] Verner D A and Yakovelev D G 1993 *At. Data Nucl. Data Tables* **55** 233

[39] Sardar S, Bilal M, Nazir R T, Bari M A, Hannan A and Nasim M H 2015 *MNRAS* **450** 1631

[40] Del Zanna G and Storey P J 2013 *Astron. Astrophys.* **549** A42

[41] Biémont E and Hansen J E 1986 *Phys. Scr.* **34** 116

[42] Träbert E, Saathoff G and Wolf A 2004 *Eur. Phys. J. D* **30** 297

[43] Träbert E, Hoffmann J, Krantz C, Wolf A, Ishikawa Y and Santana J A 2009 *J. Phys. B: At. Mol. Opt. Phys.* **42** 025002

[44] Träbert E, Grieser M, Krantz C, *et al.* 2012 *J. Phys. B: At. Mol. Opt. Phys.* **45** 215003

[45] Träbert E, Calamai A G, Gwinner G, *et al.* 2003 *Phys. B: At. Mol. Opt. Phys.* **36** 1129

[46] Kaufman B and Sugar J 1986 *J. Phys. C. Ref. Data* **15** 321